
Behaviour Discovery and Attribution for Explainable Reinforcement Learning

Rishav Rishav^{1,2} Somjit Nath^{1,3} Vincent Michalski^{1,4} Samira Ebrahimi Kahou^{1,2,5}

Abstract

Explaining the decisions made by reinforcement learning (RL) agents is critical for building trust and ensuring reliability in real-world applications. Traditional approaches to explainability often rely on saliency analysis, which can be limited in providing actionable insights. Recently, there has been growing interest in attributing RL decisions to specific trajectories within a dataset. However, these methods often generalize explanations to long trajectories, potentially involving multiple distinct behaviors. Often, providing multiple more fine-grained explanations would improve clarity. In this work, we propose a framework for behavior discovery and action attribution to behaviors in offline RL trajectories. Our method identifies meaningful behavioral segments, enabling more precise and granular explanations associated with high-level agent behaviors. This approach is adaptable across diverse environments with minimal modifications, offering a scalable and versatile solution for behavior discovery and attribution for explainable RL. Our code is public¹.

1. Introduction

Explaining the decisions made by RL agents is a critical area of research, particularly as these agents are increasingly deployed in high-stakes domains such as autonomous systems, healthcare, and finance. Transparent decision-making is essential to ensure reliability, build trust, and address safety concerns in these applications (Sutton & Barto, 2018; Arulkumaran et al., 2017). Traditional approaches to RL explainability often rely on saliency analysis, which highlights the importance of specific states, actions, or rewards (Greydanus et al., 2018). While useful, these methods often fall short of providing detailed insights into the underlying decision-making processes of RL agents, especially in

dynamic environments characterized by complex and multi-faceted trajectories.

Techniques such as LIME (Ribeiro et al., 2016) and SHAP (Lundberg & Lee, 2017) offer model-agnostic frameworks for interpreting decisions by attributing them to input features, and these approaches have been extended to RL contexts (Beechey et al., 2023). Another line of work explore trajectory-level attribution by associating an agent’s current decisions with past experiences (Madumal et al., 2020). More recently, Deshmukh et al. (2024) developed a mechanism to attribute RL decisions to specific trajectories within a dataset. However, most trajectory-based methods treat trajectories as singular units, disregarding the fact that they often encapsulate multiple distinct behaviors. This limitation can lead to diluted or ambiguous explanations, making it difficult to align decisions with meaningful, high-level behavioral patterns.

To address these challenges, we propose a novel framework that first performs behavior discovery within offline RL trajectories and subsequently attributes RL decisions to specific *behaviors* rather than the trajectory as a whole. By isolating and focusing on these high-level behaviors, our framework provides precise and interpretable insights into the decision-making processes of RL agents. The framework’s two-stage approach ensures that behavior discovery lays the foundation for accurate attribution, making it both adaptable across diverse RL environments and inherently scalable to more complex tasks.

Our framework is composed of three interconnected components. The first component employs a Vector Quantized Variational Autoencoder (VQ-VAE) (Oord et al., 2017) to quantize sequences of states and actions into discrete tokens. The resulting discrete codes are treated as representations of micro and macro behaviors within the trajectories. The second component first builds a graph where nodes represent the codebook vectors and edges capture their behavioral similarity based on the euclidean distance and the transition probability. Then, using spectral clustering graph cut, the graph is partitioned to identify distinct clusters of behaviors, isolating meaningful patterns from the data. The final component aligns these isolated behaviors with RL agent decisions, providing targeted and interpretable attributions for each action.

¹Mila - Quebec AI Institute ²University of Calgary ³McGill University ⁴University of Montreal ⁵CIFAR AI Chair. Correspondence to: Rishav Rishav <mail.rishav9@gmail.com>.

¹<https://rish-av.github.io/bexrl>

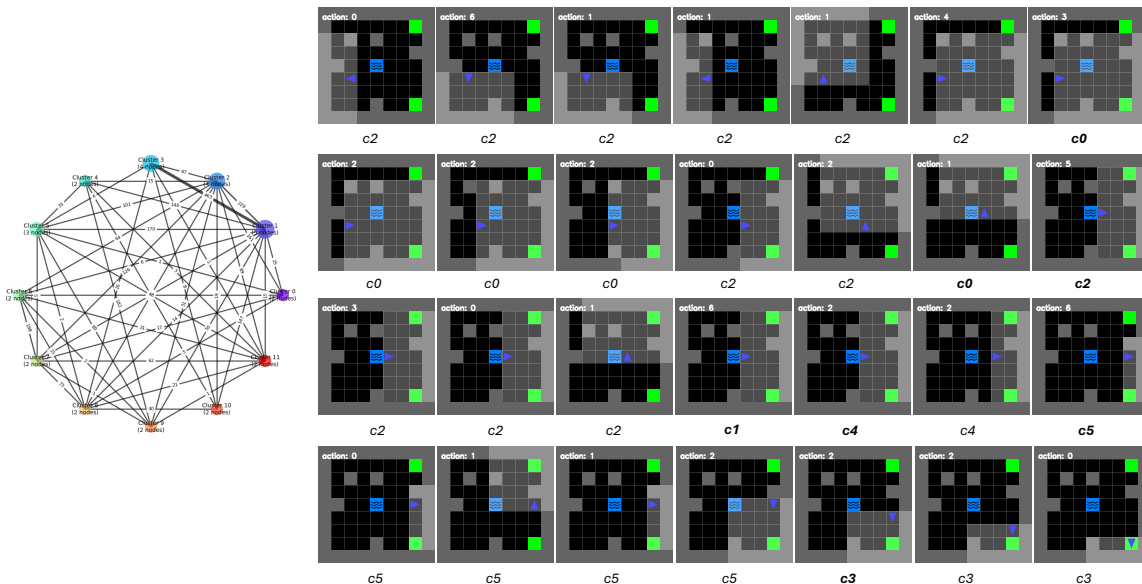


Figure 1. Using our pipeline, behavior segmentation reveals distinct clusters, each corresponding to specific patterns in the agent’s actions. In this figure (best viewed at 250% zoom), we present the behavior graph and a sample sequence for MiniGridTwoGoalsLava environment where **cx** below each figure represents its cluster classification. Here cluster 2 comprises scenarios where the agent is exploring the environment. Cluster 0 corresponds to cases when the agent is crossing the lava and cluster 3 to the case when the agent is approaching the goal. For all other definitions, please refer to Table 1.

By combining these components, our framework addresses the limitations of existing trajectory-based attribution methods (Deshmukh et al., 2024), offering a detailed and behavior-focused understanding of RL agent actions. The modular and adaptable design of the framework ensures its applicability across a wide range of RL tasks, supporting the development of more transparent and trustworthy RL systems.

Figure 1 illustrates the segmentation of behaviors within trajectories for a minigrid environment. Each cluster of state transitions corresponds to a distinct behavior. When the agent performs an action, we can use a similarity measure to attribute that action into a specific behavior cluster. This approach promotes explainable decision-making by mapping actions to identifiable behaviors.

Overall, our main contributions include a novel framework to isolate behaviors from RL trajectories and subsequently attributing actions taken by policies trained on the entire dataset to these learned behaviors. We verify the effectiveness of our framework on dataset from three major environments where we successfully isolate high-level behaviors and perform attribution on randomly selected actions.

2. Related Work

Behavior Discovery in RL: Behavior discovery in RL has primarily been driven by the goal of extracting reusable

skills to improve transfer learning and hierarchical policy learning. Early work on options (Sutton et al., 1999; Precup, 2000) introduced temporally extended actions that allow agents to plan at multiple levels of abstraction. Subsequent methods (Bacon et al., 2017; Harb et al., 2017; Bagaria & Konidaris, 2020; Barreto et al., 2021; Jin et al., 2022), focused on learning options from intrinsic rewards and clustering state transitions to discover meaningful sub-policies. More recent approaches in unsupervised skill discovery use information-theoretic objectives (Eysenbach et al., 2018; Achiam et al., 2018) to learn diverse behaviors without task-specific rewards. Bayesian nonparametric skill discovery (Villego et al., 2022) further removes the need to pre-define the number of skills, making skill learning more adaptive. However, most of these methods are designed for online RL, where agents actively interact with the environment, limiting their applicability in offline RL, where data is fixed.

In offline RL, where skill discovery is performed on fixed datasets, several methods have been proposed to extract latent behavior structures. OPAL (Ajay et al., 2021) learns a continuous space of behavior embeddings that accelerate policy learning while ensuring actions remain within the dataset distribution. Generative models such as high-fidelity behavior modeling (Chen et al., 2022) use diffusion-based priors to model realistic trajectories and avoid out-of-distribution errors. Other works focus on skill segmentation through clustering techniques (Zhang & Kashima, 2023)

or by organizing discovered skills into structured graphs (ya Halevy et al., 2023), enabling compositional planning. While these methods successfully compress behavior representations for policy optimization, they are primarily aimed at enhancing generalization and transfer learning, rather than producing human interpretable behaviors.

In contrast, our approach leverages a VQ-VAE (Oord et al., 2017) trained on offline state-action sequences to discover behaviors without relying on predefined heuristics. We utilize the strong representation capabilities of transformers to discretize long-range sequences and later use a graph-cut approach to segment behaviors. Furthermore, we provide an attribution framework where we attribute actions taken by a policy trained on the entire dataset to the segmented behaviors.

Explainability in Reinforcement Learning (XRL): Explainability in RL is crucial for addressing the opacity of black-box policies. Existing methods primarily identify and visualize features that influence an agent’s decisions. Saliency-based techniques, such as those by Huber et al. (2021), highlight critical input regions, while attention mechanisms assign importance scores to state elements. Visualization methods, including activation maps and trajectory heatmaps (Zahavy et al., 2017; Greydanus et al., 2018), reveal behavioral patterns but struggle with high-dimensional or abstract state spaces.

Policy summarization approaches, such as PIRL (Verma et al., 2019), approximate policies with rule-based models, while reward decomposition (Juozapaitis et al., 2019) breaks total rewards into interpretable components. However, these methods operate at the trajectory level, limiting their ability to analyze fine-grained behaviors. Model-based approaches improve interpretability through counterfactual reasoning. Causal models (Madumal et al., 2020) analyze alternative trajectories, and causal inference techniques (Seitzer et al., 2021) identify key decision-driving state variables. While effective, these methods rely on structured assumptions and lack mechanisms to isolate distinct behaviors within trajectories.

Trajectory-based attribution (Deshmukh et al., 2024) assumes decisions are influenced by entire trajectories but lacks behavioral granularity. In contrast, our transformer-based VQ-VAE framework attributes decisions to isolated high-level behaviors. By integrating vector quantization with graph-based segmentation, we learn discrete behavior representations that capture temporal coherence while enabling structured, fine-grained behavior attribution. This bridges the gap between local action relevance and high-level policy summarization, improving interpretability beyond existing methods.

Vector Quantization in RL Vector Quantization (VQ)

methods have been applied in RL to discretize continuous state, action, and trajectory representations into structured codebooks. This discretization facilitates efficient learning, improves exploration, and enhances interpretability. SAQ (Luo et al., 2023) used a VQ-VAE based framework to discretize action in environments with large continuous actions. Their approach demonstrated that quantized representations could improve exploration by balancing abstraction and granularity.

Hierarchical reinforcement learning has also benefited from quantization techniques. Nachum et al. (2018) employed discrete representations for value function approximation, enabling structured learning of sub-policies within large state spaces. In model-based RL, Hafner et al. (2020) utilized vector quantization in the latent space to improve long-term planning by discretizing learned latent variables. This approach allowed agents to reason about behaviors efficiently over extended time horizons while maintaining a compact representation of the environment.

Our approach uses a transformer-based VQ-VAE to obtain discrete representations of long-range sequences, which are then used to construct a graph. By applying a graph-cut method, we isolate distinct high-level behaviors. Explicitly modeling these high-level behaviors enhances the granular understanding of decision-making processes, improving both the interpretability and scalability of RL models in complex environments.

3. Method

3.1. Behavior Discovery

Behavior discovery is at the core of our framework where we identify and segment meaningful sub-trajectories from offline RL data. Our framework employs a Vector Quantized Variational Autoencoder (VQ-VAE) trained in a sequence-to-sequence fashion, the output of which is then used by a graph-cut algorithm to isolate behaviors.

The architecture begins with a transformer-based encoder that processes sequences of state-action pairs

$$\{(s_t, a_t), (s_{t+1}, a_{t+1}), \dots, (s_{t+k}, a_{t+k})\},$$

where $s_t \in \mathbb{R}^n$ ($s \in \mathbb{R}^{n \times n}$ for image based states) and $a_t \in \mathbb{R}^m$ where n and m are the state and action space dimensions respectively. Positional encodings are added to retain temporal order, and a causal mask is applied to ensure that future information is not used during encoding. The encoder maps the input sequence to a latent representation $z_t \in \mathbb{R}^d$, capturing the temporal relationships within the data.

The latent representations z_t are then discretized using vec-

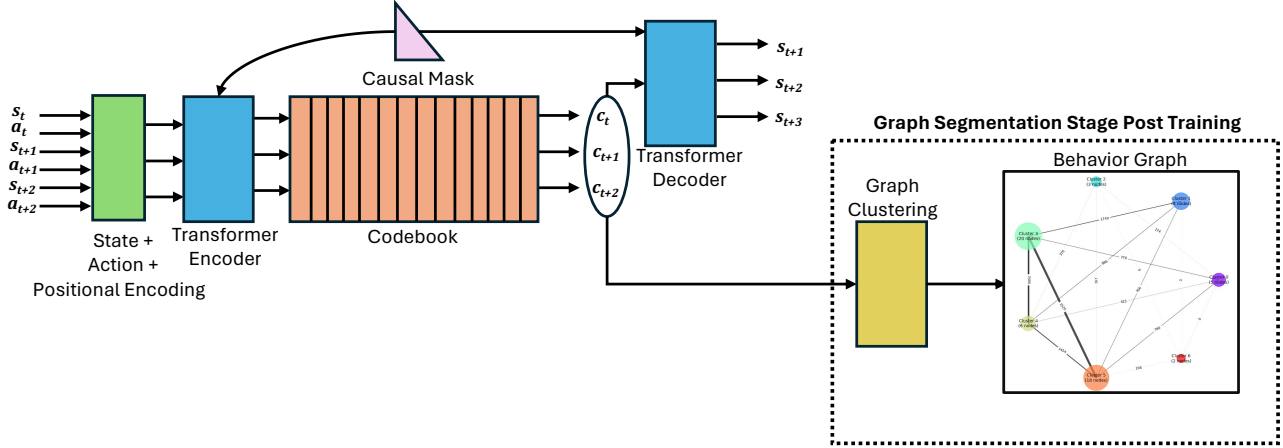


Figure 2. A transformer-based VQ-VAE is used for behavior discovery, where state-action sequences are encoded, discretized via a codebook, and decoded to predict future states. The resulting latent codes are used to construct a graph, and the graph clustering module partitions the graph into subgraphs, each representing a “behavior”. A causal mask is applied to both the decoder and the encoder to restrict access to future information.

tor quantization. A learnable codebook

$$\mathcal{C} = \{c_1, c_2, \dots, c_N\}$$

maps each z_t to the nearest codebook vector c_q , determined by:

$$q(z_t) = \arg \min_{c_i \in \mathcal{C}} \|z_t - c_i\|^2.$$

This discretization step enables the model to cluster latent representations into discrete categories, facilitating the identification of meaningful behaviors. The vector quantization process is optimized using a combination of codebook and commitment losses:

$$\mathcal{L}_{\text{vq}} = \mathbb{E} [\|z_t - \text{sg}(c_q)\|^2] + \mathbb{E} [\|\text{sg}(z_t) - c_q\|^2],$$

where $\text{sg}(\cdot)$ denotes the stop-gradient operation.

Once discretized, the latent codes c_q are passed to the decoder, which reconstructs future states

$$\{\hat{s}_{t+1}, \hat{s}_{t+2}, \dots\}.$$

The decoder also uses a causal mask to ensure that only past information is used during reconstruction. The model is trained end-to-end by minimizing a combination of the reconstruction loss and the vector quantization loss:

$$\mathcal{L} = \mathcal{L}_{\text{recon}} + \alpha \mathcal{L}_{\text{vq}},$$

where $\mathcal{L}_{\text{recon}}$ measures the error between the predicted and actual states:

$$\mathcal{L}_{\text{recon}} = \mathbb{E} \left[\sum_{t=1}^k \|s_t - \hat{s}_t\|^2 \right].$$

Despite its effectiveness in capturing temporal dependencies, the VQ-VAE discretization process introduces variability, as each latent representation encodes information from its past inputs. This can lead to inconsistencies in segmentation, where similar behaviors may be assigned different codes due to minor variations in the input sequences. Additionally, we want semantically similar codebook vectors to be grouped together to ensure meaningful clustering. To achieve this, we employ a graph-based segmentation approach, which refines the behavior clusters by incorporating both transition frequencies and latent-space proximity. The details of this approach are described next.

3.2. Behavior Segmentation

To segment meaningful behaviors from offline RL data, we employ a graph-based approach. The key idea is to construct a graph where nodes represent discrete latent codes obtained from vector quantization, and edges encode transition relationships. A graph partitioning technique is then used to identify distinct behavioral patterns.

Formally, we construct a graph $G = (V, E)$, where each node $v_i \in V$ corresponds to a codebook vector c_i obtained from the behavior discovery phase. The edge weights w_{ij} between two nodes c_i and c_j are defined as:

$$w_{ij} = \text{Count}(c_i \rightarrow c_j) + \lambda \|c_i - c_j\|_2^2,$$

where $\text{Count}(c_i \rightarrow c_j)$ denotes the normalized frequency of transitions from c_i to c_j in the dataset, and the term $\lambda \|c_i - c_j\|_2^2$ ensures that behaviors with similar representations are grouped together. The hyperparameter λ controls the trade-

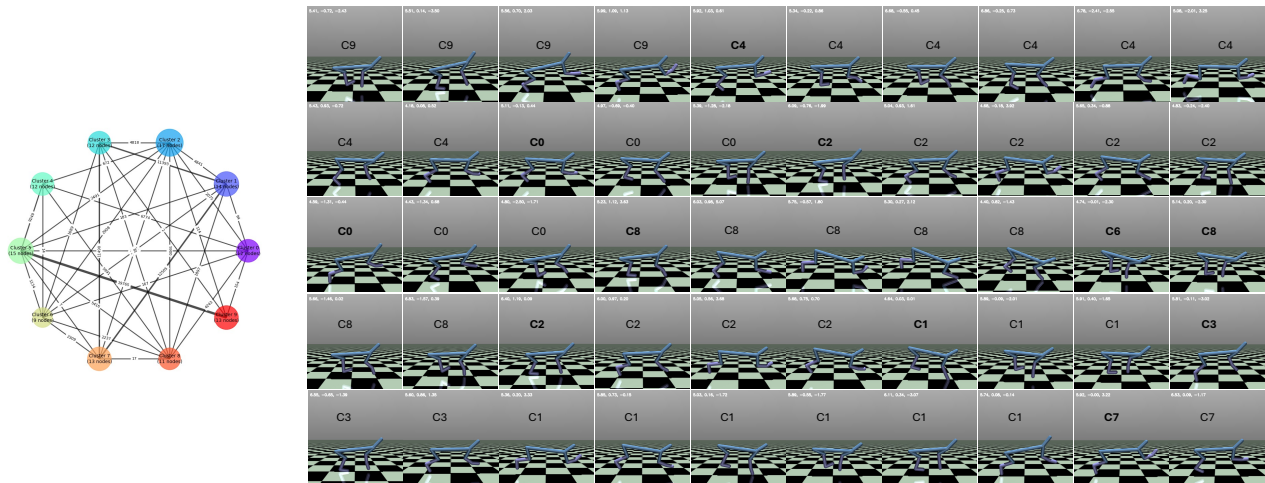


Figure 3. A sample sequence from HalfCheetah with cluster labels and the corresponding segmentation graph (the image is best viewed at 250% zoom), \mathbf{c}_x in the center of each figure represents its cluster classification. For instance, in this sample, Cluster 0 comprises scenarios where the cheetah is preparing to jump by exerting force on its hind-legs. Cluster 1 has the cases where the cheetah is running on its front legs while mildly accelerating, Cluster 2 corresponds “leaping forward” behavior. Descriptions of other clusters alongside the behavior graph can be found in A.

off between transition frequency and spatial regularization. We ablate λ in Section B.1.

The motivation behind incorporating both transition frequencies and spatial proximity in defining edge weights stems from the nature of macro behaviors, which typically persist over multiple timesteps. Relying solely on transition counts can be problematic: in some cases, it may lead to over-segmentation, where minor variations cause a single behavior to be split into multiple clusters, and in other cases, it may result in under segmentation, where high transition counts between distinct behaviors cause them to be merged. Conversely, using only spatial proximity might overlook important temporal consistencies. By combining these factors, the segmentation approach captures both temporal coherence and structural similarity in the learned latent representations.

Thus, given this graph representation, we apply spectral clustering to partition the nodes into behaviorally distinct groups. Spectral clustering is particularly suitable here as it effectively captures the global structure of the graph and allows for flexible, non-convex clusters, which aligns with the nature of behavioral patterns in RL.

The segmentation process begins by computing the similarity matrix S , where the similarity between nodes i and j is given by:

$$S_{ij} = w_{ij} + w_{ji}.$$

Next, the Laplacian matrix L is defined as:

$$L = D - S,$$

where D is the degree matrix with diagonal entries $D_{ii} = \sum_j S_{ij}$. The top k eigenvectors corresponding to the smallest non-zero eigenvalues of L are used to embed the nodes into a lower-dimensional space, where they are clustered using k -means. The number of clusters k is determined by identifying the largest eigenvalue gap in the Laplacian spectrum.

Each cluster represents a unique behavior, and trajectory segments are labeled accordingly. This segmentation approach ensures that behaviors are temporally coherent and structurally meaningful, providing a robust representation of the underlying dynamics in offline RL data.

3.3. Attributing Actions to Behaviors

Attributing actions taken by the policy trained on entire dataset to learned behaviors provides insight into the origins of specific decisions made by a policy. This process helps in understanding which behaviors contribute to particular actions and where they were learned from. To achieve this, we train a policy π on the entire dataset while also training separate behavior cloning models M_k for each discovered behavior k using the trajectory segments associated with that cluster. During inference, we attribute an observed action to the most relevant behavior by comparing the policy’s output with the predictions from each behavior model.

The method of attribution depends on whether the action

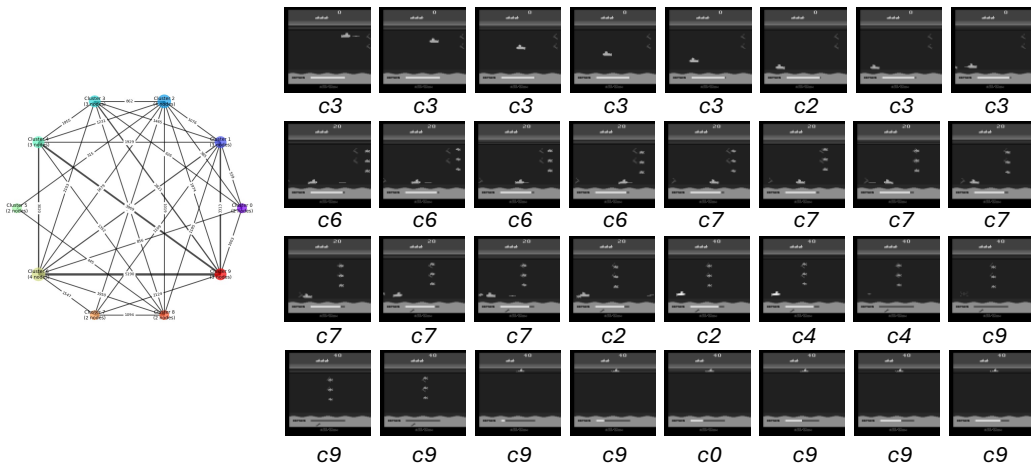


Figure 4. A sample sequence from Seaquest-mixed-v0 with cluster labels and the corresponding segmentation graph (the image is best viewed at 250% zoom), \mathbf{cx} under each figure represents its cluster classification. For instance, in this sample, Cluster 3 comprises scenarios where the agent is moving downwards. Cluster 6 is when the agent is moving to the right, Cluster 7 corresponds to the case when the agent is moving leftwards and Cluster 9 is when the agent is filling oxygen. Descriptions of other clusters can be found in 1.

space is continuous or discrete. In continuous action spaces, we compute the mean squared error (MSE) between the observed action $\pi(s) = a$ and the action \hat{a}_k predicted by each behavior model M_k . The behavior k^* is attributed as follows:

$$k^* = \arg \min_k \text{MSE}(a, \hat{a}_k),$$

where

$$\text{MSE}(a, \hat{a}_k) = \frac{1}{d} \sum_{i=1}^d (a_i - \hat{a}_{k,i})^2.$$

Here, d is the dimensionality of the action space, a_i is the i -th dimension of the observed action, and $\hat{a}_{k,i}$ is the i -th dimension of the action predicted by model M_k .

In discrete action spaces, we compare the probability distribution p_k predicted by each behavior model M_k over the action space with the observed action probability distribution p_a . To measure similarity, we compute the cross-entropy between p_a and p_k . The behavior k^* is attributed as follows:

$$k^* = \arg \min_k \mathcal{L}_{\text{CE}}(p_a, p_k),$$

where the cross-entropy loss is defined as:

$$\mathcal{L}_{\text{CE}}(p_a, p_k) = - \sum_{j=1}^C p_{a,j} \log(p_{k,j}).$$

Here, C is the number of discrete actions.

Some examples of this attribution pipeline can be found in Table 5.

4. Experiments

We evaluated the effectiveness of our framework for behavior discovery and attribution using two benchmark environments from D4RL (D4RL): Seaquest-Mixed-v0 and HalfCheetah-Medium-v2. Additionally, we developed a Minigrid Environment featuring a lava obstacle and two distinct goals, which enabled us to better characterize and visualize diverse behaviors. We’ve named this environment MiniGridTwoGoalsLava. These environments were selected for their diversity in state-action spaces and varying levels of complexity, enabling us to test the framework’s ability to generalize across discrete and continuous domains. The offline datasets comprised trajectories generated by partially trained agents (using PPO Schulman et al. (2017) upto 1/3 of best performance), reflecting real-world mix of optimal and sub-optimal behaviors. Our pipeline, which utilizes a transformer-based VQ-VAE model, discretized state-action sequences into latent codes that effectively capture the dynamics of each environment. Using these latent codes, we constructed a graph with nodes and then used spectral clustering to obtain segmented trajectories as described in section 3.2. We also conducted an extensive ablation with various codebook sizes, the details of which are provided in B.1. We list the set of hyper-parameters and training details in Appendix C.

Cluster #	HalfCheetah-medium-v2	MiniGridTwoGoalsLava	Seaquest-mixed-v0
0	Jump prep using hind legs	Crossing lava	Exploration Variety
1	Running on hind legs	Running into obstacle/wall	Exploration Variety
2	Leaping forward, decelerating	Exploration Variety	Transition stage
3	Gait transition, braking	Approaching/landing on goals	Moving downwards
4	Bounding motion, slight accel.	Forward motion with exploration	Agent killed
5	Falling-driven bounding	Stuck at obstacle/wall	Firing randomly from same location
6	Falling with Recovery	Continuous forward motion	Moving right
7	Leaping, accelerating	Transition stage	Moving left
8	Bounding gait	Exploration within grid	Exploration variety
9	Initial states of sequence	Transition stage	Filling oxygen
10	–	Exploration around corners	–
11	–	Continuous exploration (not stuck)	–

Table 1. List of behaviors found in each of the environments. One noticeable point is the existence of multiple exploration clusters, this is a consequence of datasets derived from sub-optimal policies since agents still have high exploration tendencies.

4.1. Behavior Discovery and Segmentation

Our framework demonstrated its ability to identify and segment meaningful behaviors across all environments. These behaviors were captured by the constructed graph, with spectral clustering isolating coherent subgraphs that align with intuitive behavioral patterns observed in the trajectories. The similarity matrix, based on transition frequency and spatial proximity, ensured that clusters reflected both temporal and spatial coherence.

Our approach can effectively distinguish between various agent behaviors, yielding distinct behavior clusters. Each of the clusters represent an unique behavior as portrayed in Table 1. This clear separation of behaviors within each cluster demonstrates the environment’s capacity to provide a nuanced understanding of the agent’s actions. For example for MiniGrid, we can see distinct behaviors for crossing lava, exploration near the wall and approaching the goal. In Seaquest-Mixed-v0, the framework identified distinct behaviors such as frequent shooting, obstacle avoidance, and navigation toward specific regions. In HalfCheetah-Medium-v2, behaviors such as slow walking, high-speed running, and transitions leading to instability were effectively clustered.

In Figures 1, 3, & 4, we again visualize this with the help of a sequence from the training dataset, where we clearly see the clusters changing as the agent changes behaviors within the episode. What makes this approach particularly compelling is its ability to track behavioral shifts at an action-level granularity, meaning cluster assignments change instantaneously when an agent’s action deviates from the cluster’s defining characteristics. This granular clustering not only provides insights into the agent’s decision-making process but also highlights the sophisticated adaptability of the behavioral segmentation framework.

4.2. Behavior Attribution

To validate the discovered behaviors, we trained behavior cloning models for each identified cluster, enabling the attribution of specific actions to their corresponding behaviors. For continuous action spaces, such as in HalfCheetah-Medium-v2, attribution was performed by minimizing the mean squared error (MSE) between observed and predicted actions, while in discrete environments, such as Seaquest-Mixed-v0 and MiniGridTwoGoalsLava, cross-entropy loss was used to compare predicted action distributions against observed actions. Across all environments, the attribution process demonstrated high accuracy, with behaviors aligning well with agent decisions. For instance, in Seaquest-Mixed-v0, shooting sequences were consistently attributed to their corresponding cluster, while in HalfCheetah-Medium-v2, distinct clusters captured high-speed accelerations and slower, stable transitions. These results highlight the framework’s capability to attribute actions to interpretable behavioral patterns, providing actionable insights into agent decision-making processes. Some attribution examples can be found in Figure 5.

5. Limitations

The proposed framework, while effective in discovering and attributing behaviors, has certain limitations that warrant consideration. In highly stochastic environments, overlapping or ambiguous behaviors can result in less distinct segmentation, particularly when transitions between behaviors are frequent or noisy as observed in HalfCheetah. While segmentation is clean and most behavior clusters are meaningful, it is sometimes hard to visually verify what some clusters signify as in the case of Cluster 5 in MiniGridTwoGoalsLava. Additionally, the graph segmentation relies on traditional cut approaches. We propose exploring graph

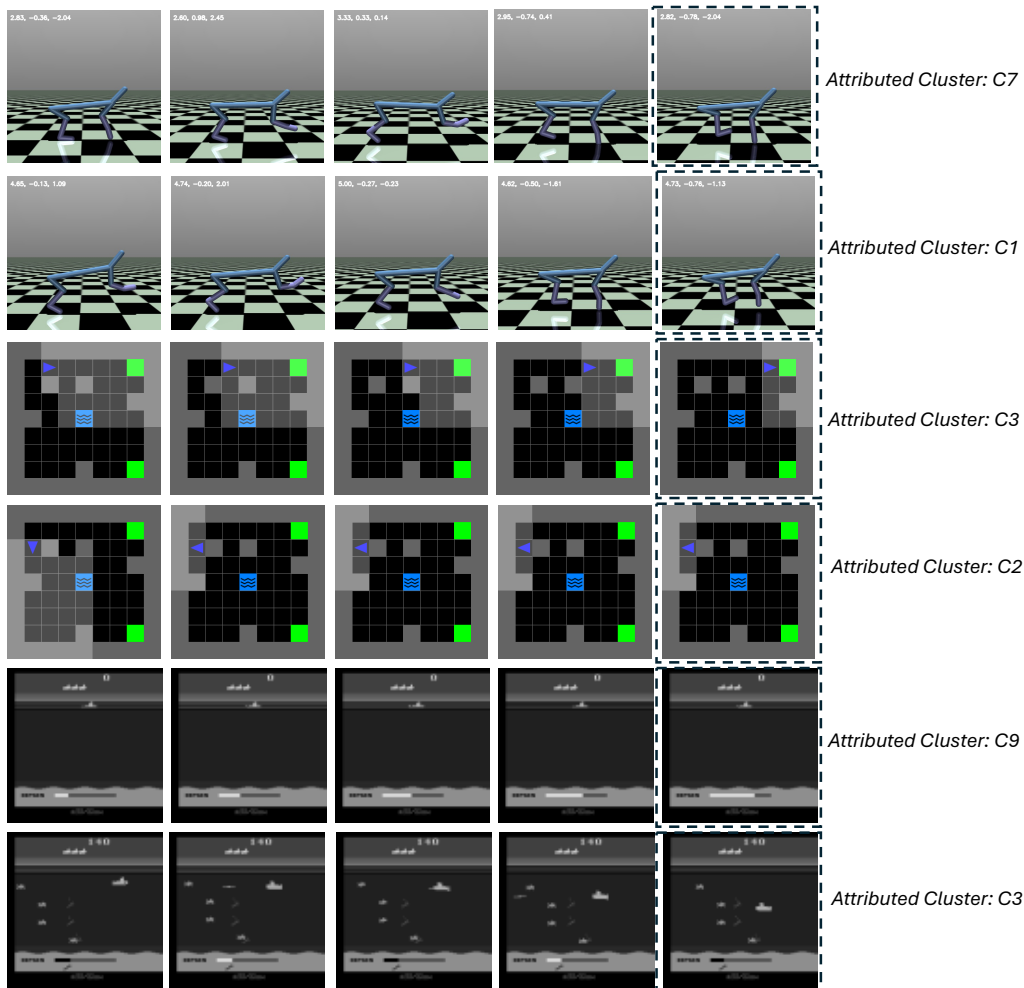


Figure 5. Attribution results for various environments, the attribution as described in Section 3.3 is done for the last frame in the shown sequences. However, to provide better historical context, we have also added some previous frames. The attribution results for Mujoco is consistent with the behaviors we have listed out in A. For instance, the cheetah is running on the hind legs for the sample that got attributed to Cluster 1. Similarly, it shows leaping motion for the case where the sample was attributed to Cluster 7.

neural network based approaches for segmentation as future work.

6. Conclusion

This work proposed a framework for behavior discovery and attribution in offline reinforcement learning, using a transformer-based VQ-VAE to encode state-action sequences into discrete latent representations and graph-based segmentation to identify macro-level behaviors. Spectral clustering enabled the partitioning of trajectories into temporally coherent, interpretable subgraphs, providing a granular understanding of agent decision-making. Experiments across Seaquest-Mixed-v0, HalfCheetah-Medium-v2, and MiniGridTwoGoalsLava demonstrated the framework’s generalization to discrete and continuous action spaces, effectively isolating and attributing distinct behaviors. Quanti-

tative evaluations highlighted the importance of codebook size in balancing segmentation quality and computational efficiency. While challenges remain in highly stochastic environments, the framework offers a scalable approach to explainable reinforcement learning, with future work addressing these limitations and exploring real-time applications.

7. Impact Statement

This paper presents work whose goal is to advance the field of Machine Learning. There are many potential societal consequences of our work, none which we feel must be specifically highlighted here.

8. Acknowledgment

We sincerely thank NSERC, CIFAR, Digital Research Alliance of Canada & Denvr Datacloud for providing resources to complete this project.

References

- Achiam, J., Edwards, H., Amodei, D., and Abbeel, P. Variational option discovery algorithms, 2018. URL <https://arxiv.org/abs/1807.10299>.
- Ajay, A., Kumar, A., Agrawal, P., Levine, S., and Nachum, O. Opal: Offline primitive discovery for accelerating offline reinforcement learning. In *International Conference on Learning Representations (ICLR)*, 2021. URL <https://openreview.net/forum?id=V69LGwJ01IN>.
- Arulkumaran, K., Deisenroth, M. P., Brundage, M., and Bharath, A. A. Deep reinforcement learning: A brief survey. *IEEE Signal Processing Magazine*, 34(6):26–38, 2017.
- Bacon, P.-L., Harb, J., and Precup, D. The option-critic architecture. In *Proceedings of the AAAI conference on artificial intelligence*, volume 31, 2017.
- Bagaria, A. and Konidaris, G. D. Option discovery using deep skill chaining. In *International Conference on Learning Representations*, 2020. URL <https://api.semanticscholar.org/CorpusID:209450128>.
- Barreto, A., Borsa, D., Hou, S., Comanici, G., Aygün, E., Hamel, P., Toyama, D., Hunt, J. J., Mourad, S., Silver, D., and Precup, D. The option key-board: Combining skills in reinforcement learning. In *Neural Information Processing Systems*, 2021. URL <https://api.semanticscholar.org/CorpusID:202764647>.
- Beechey, D., Smith, T. M., and Şimşek, Ö. Explaining reinforcement learning with shapley values. In *International Conference on Machine Learning*, pp. 2003–2014. PMLR, 2023.
- Chen, H., Lu, C., Ying, C., Su, H., and Zhu, J. Offline reinforcement learning via high-fidelity generative behavior modeling. *arXiv preprint arXiv:2209.14548*, 2022. URL <https://arxiv.org/abs/2209.14548>.
- Deshmukh, S. V., Dasgupta, A., Krishnamurthy, B., Jiang, N., Agarwal, C., Theodorou, G., and Subramanian, J. Explaining rl decisions with trajectories, 2024. URL <https://arxiv.org/abs/2305.04073>.
- Eysenbach, B., Gupta, A., Ibarz, J., and Levine, S. Diversity is all you need: Learning skills without a reward function, 2018. URL <https://arxiv.org/abs/1802.06070>.
- Greydanus, S., Koul, A., Dodge, J., and Fern, A. Visualizing and understanding atari agents. In *Proceedings of the International Conference on Machine Learning (ICML)*, 2018.
- Hafner, D., Lillicrap, T., Ba, J., and Norouzi, M. Dream to control: Learning behaviors by latent imagination. In *International Conference on Learning Representations (ICLR)*, 2020.
- Harb, J., Bacon, P.-L., Klissarov, M., and Precup, D. When waiting is not an option : Learning options with a deliberation cost, 2017. URL <https://arxiv.org/abs/1709.04571>.
- Huber, T., Weitz, K., André, E., and Amir, O. Local and global explanations of agent behavior: Integrating strategy summaries with saliency maps. *Artificial Intelligence*, 301:103571, 2021.
- Jin, M., Ma, Z., Jin, K., Zhuo, H. H., Chen, C., and Yu, C. Creativity of ai: Automatic symbolic option discovery for facilitating deep reinforcement learning. *ArXiv*, abs/2112.09836, 2022. URL <https://api.semanticscholar.org/CorpusID:245335262>.
- Juozapaitis, Z., Koul, A., Fern, A., et al. Explainable reinforcement learning via reward decomposition. In *Proceedings of the 28th International Joint Conference on Artificial Intelligence (IJCAI)*, 2019.
- Lundberg, S. M. and Lee, S.-I. A unified approach to interpreting model predictions. In *Advances in Neural Information Processing Systems (NeurIPS)*, pp. 4765–4774, 2017.
- Luo, J., Dong, P., Wu, J., Kumar, A., Geng, X., and Levine, S. Action-quantized offline reinforcement learning for robotic skill learning. 2023. URL <https://openreview.net/forum?id=n91ew97SAn>.
- Madumal, P., Miller, T., Sonenberg, L., and Vetere, F. Explainable reinforcement learning through a causal lens. In *Proceedings of the AAAI Conference on Artificial Intelligence*, 2020.
- Nachum, O., Gu, S., Lee, H., and Levine, S. Near-optimal representation learning for hierarchical reinforcement learning. In *International Conference on Learning Representations (ICLR)*, 2018.

- Oord, A. v. d., Vinyals, O., and Kavukcuoglu, K. Neural discrete representation learning. In *Advances in Neural Information Processing Systems (NeurIPS)*, pp. 6306–6315, 2017.
- Precup, D. *Temporal abstraction in reinforcement learning*. University of Massachusetts Amherst, 2000.
- Ribeiro, M. T., Singh, S., and Guestrin, C. "why should i trust you?": Explaining the predictions of any classifier. In *Proceedings of the 22nd ACM SIGKDD International Conference on Knowledge Discovery and Data Mining (KDD)*, pp. 1135–1144. ACM, 2016.
- Schulman, J., Wolski, F., Dhariwal, P., Radford, A., and Klimov, O. Proximal policy optimization algorithms. *arXiv preprint arXiv:1707.06347*, 2017.
- Seitzer, M., Schölkopf, B., and Martius, G. Causal influence detection for improving efficiency in reinforcement learning, 2021. URL <https://arxiv.org/abs/2106.03443>.
- Sutton, R. S. and Barto, A. G. *Reinforcement Learning: An Introduction*. MIT Press, 2018.
- Sutton, R. S., Precup, D., and Singh, S. Between mdps and semi-mdps: A framework for temporal abstraction in reinforcement learning. *Artificial intelligence*, 112(1-2): 181–211, 1999.
- Verma, A., Murali, V., Singh, R., Kohli, P., and Chaudhuri, S. Programmatically interpretable reinforcement learning, 2019. URL <https://arxiv.org/abs/1804.02477>.
- Villemoore, V., Braviner, H. J., Naderian, P., Maddison, C. J., and Loaiza-Ganem, G. Bayesian nonparametrics for offline skill discovery, 2022. URL <https://arxiv.org/abs/2202.04675>.
- ya Halevy, B., Aperstein, Y., and Castro, D. D. Offline skill graph (osg): A framework for learning and planning using offline reinforcement learning skills, 2023. URL <https://arxiv.org/abs/2306.13630>.
- Zahavy, T., Zrihem, N. B., and Mannor, S. Graying the black box: Understanding dqns, 2017. URL <https://arxiv.org/abs/1602.02658>.
- Zhang, G. and Kashima, H. Behavior estimation from multi-source data for offline reinforcement learning. In *Proceedings of the AAAI Conference on Artificial Intelligence*, volume 37, pp. 11201–11209, 2023.

A. Behavior Results

A.1. MiniGridTwoGoalsLava

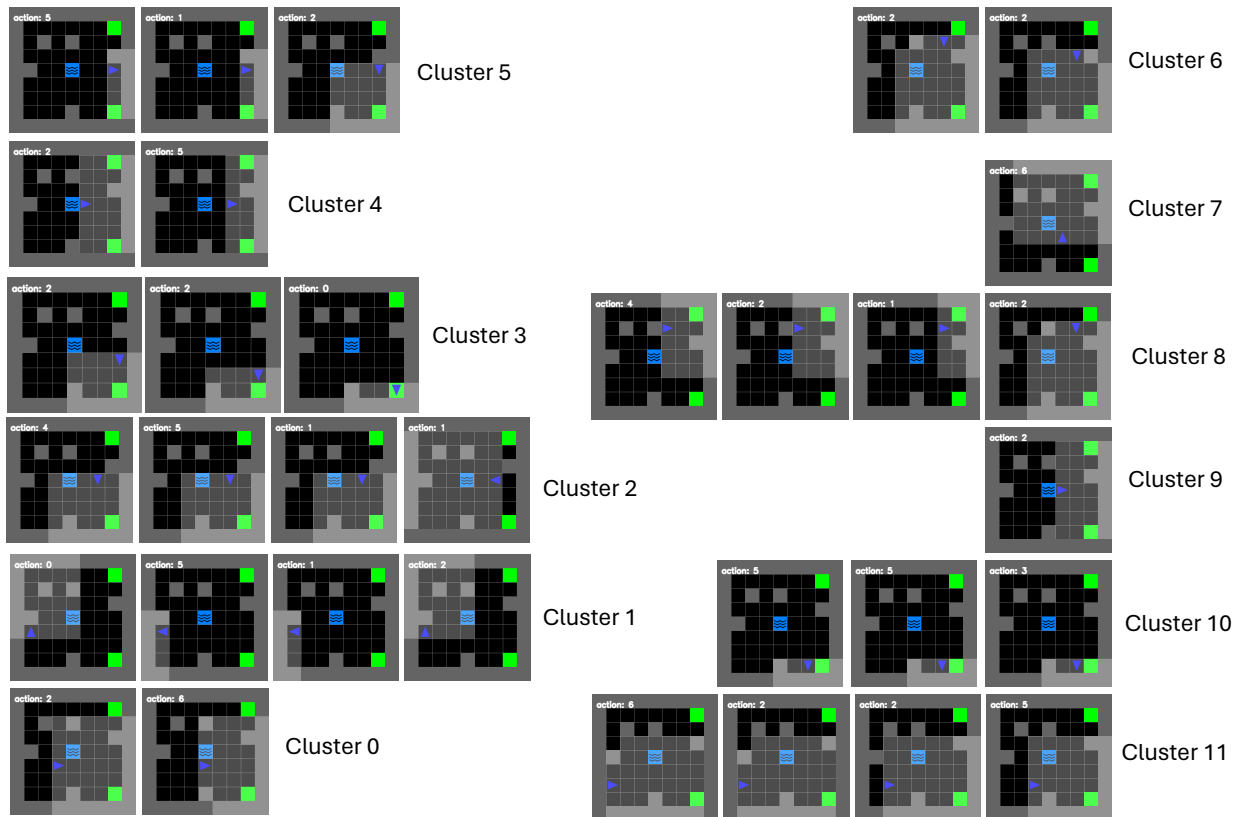


Figure 6. Different behaviors observed after segmentation of MiniGridTwoGoalsLava dataset. The segments shown here are representative of the various clusters formed. A detailed description of each is present in Table 1. The numbers on the images are the actions that were taken in that state.

A.2. Mujoco

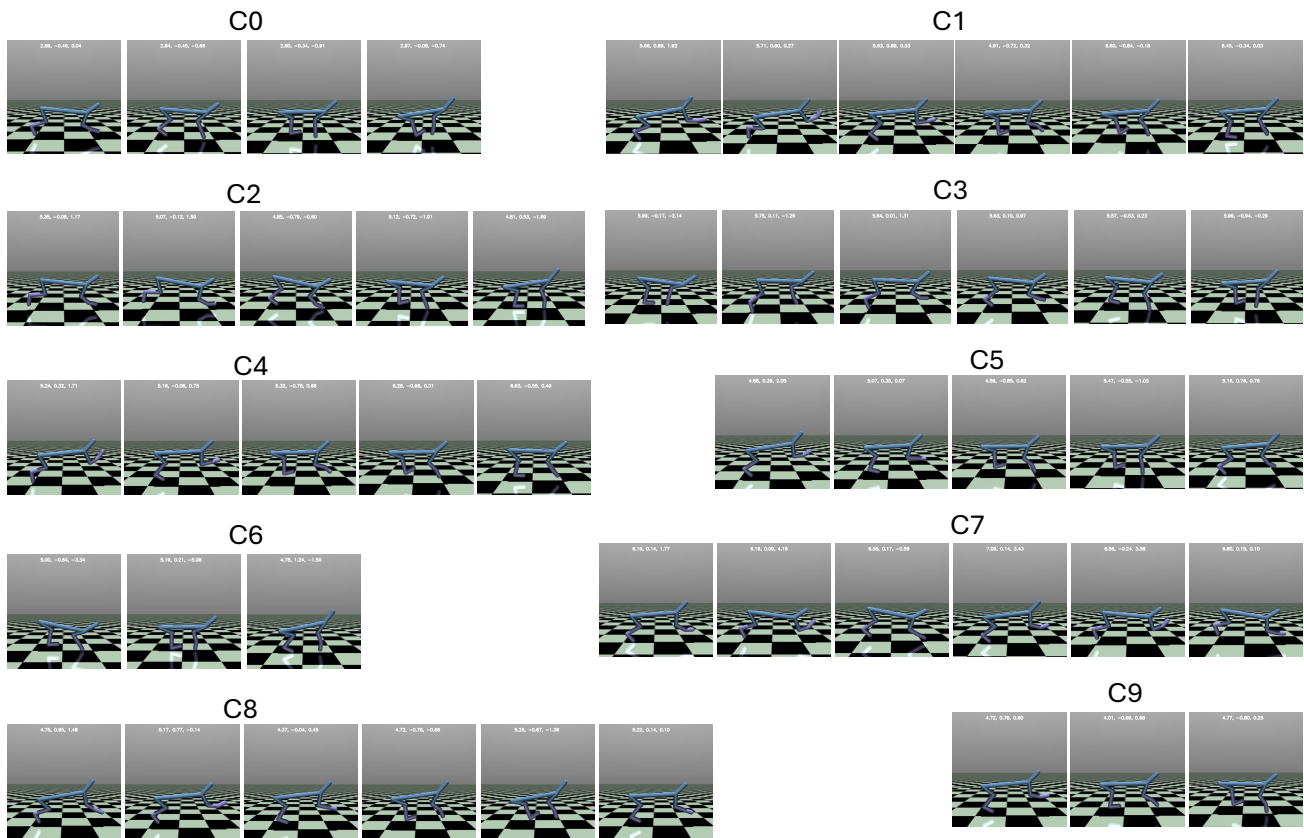


Figure 7. Different behaviors observed after segmentation of HalfCheetah-medium-v2 dataset from D4RL. The segments shown here are representative of the various clusters formed. A detailed description of each is present in Table 1. The numbers on the images are the velocities.

A.3. Seaquest-Mixed-v0

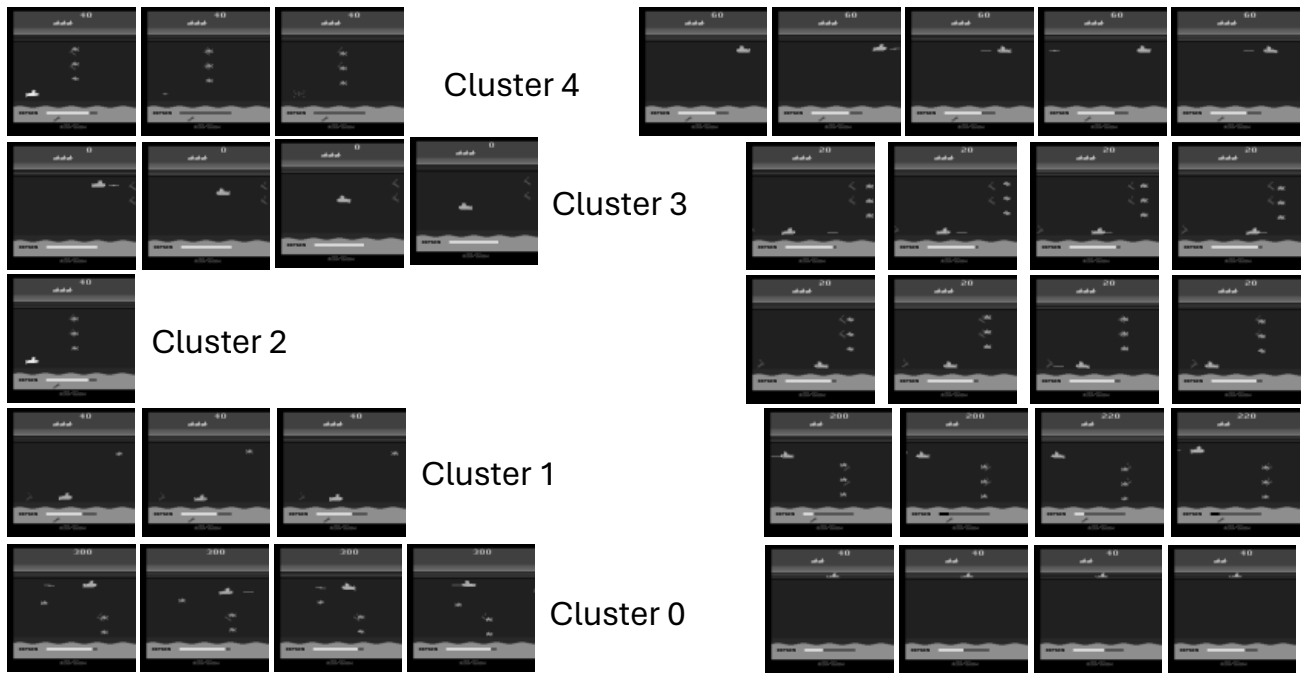


Figure 8. Different behaviors observed after segmentation of Seaquest-mixed-v0 dataset from D4RL. The segments shown here are representative of the various clusters formed. A detailed description of each is present in Table 1.

B. Ablation Study

B.1. Number of Codebooks

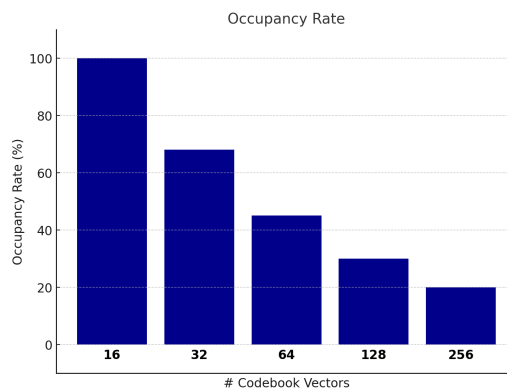


Figure 9. Occupancy rates for different number of codebooks for MiniGridTwoGoalsLava. All these variants had nearly the same reconstruction error at convergence.

We conducted an ablation study to evaluate the impact of the codebook size on behavior discovery and segmentation. We tested various codebook sizes 16, 32, 64 and 128 on MiniGridTwoGoalsLava environment. The reconstruction results were nearly consistent but the occupancy dropped for higher codebook sizes. This might be due to the fact that a lot of codebook vectors might not be needed for simple environments like MiniGridTwoGoalsLava. Thus for this environment, we decided to go with 16 vectors. To determine the optimal number of codebook vectors for a more challenging environment, we trained our architecture with HalfCheetah-medium-v2. A codebook size of 128 gave the optimal occupancy for this environment,

hence we decided to have this codebook size for challenging environments. The results of this for MiniGridLavaTwoGoals can be found in Figure 9.

B.2. Lambda Factor for Similarity Matrix

An important step in our pipeline is combining the transition probability and the euclidean distance for graph partition. Specifically for computing the similarity matrix (S , section 3.2) needed for spectral clustering. Our goal in varying this parameter was to ensure we get clusters which are human interpretable. The graph of λ vs number of clusters is presented in Figure 10 for MiniGridTwoGoalsLava. It is important to note that all values of λ might be yielding clusters which might exhibit some form of behavior. However, since our aim was to ensure the clusters formed are human interpretable, we decided to tune this hyperparameter. We performed similar experiments for HalfCheetah and Seaquest and the optimal λ for these cases turned out to be 0.7 and 0.6 respectively.

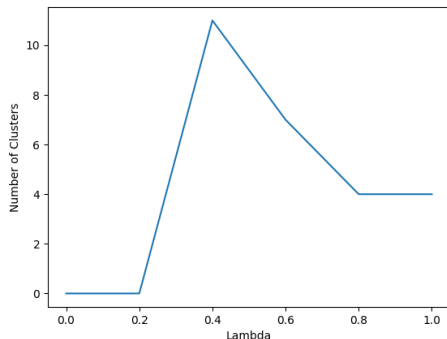


Figure 10. The maximum and most distinct clusters were obtained for $\lambda = 0.4$.

C. Hyperparameters & Training

Hyperparameter	HalfCheetah-medium-v2	MiniGridTwoGoalsLava	Seaquest-mixed-v0
Learning rate (LR)	$1e - 4$	$1e - 4$	$1e - 4$
Sequence Length (seq_len)	50	Full seqs (max 50)	60
Number of Codes (num code)	128	16	128
Embedding Dimension (embed dim)	128	128	128
Combination Param (λ)	0.7	0.4	0.6
Number of Epochs (num epochs)	50	50	50
Number of Sequences	–	900	900
Optimizer	Adam	Adam	Adam
Learning Rate Scheduler	LR	LR	LR
Frame Skip	–	–	4
Transformer Heads (num heads)	4	4	4
Encoder/Decoder Layers	4	2	4
Transformer Hidden Dimension	128	128	128

Table 2. Hyperparameter settings for HalfCheetah-medium-v2, MiniGridTwoGoalsLava, and Seaquest-mixed-v0.

We train the transformer based VQ-VAE in an end-to-end fashion with teacher forcing, the probability of which continues to decline as the training progresses.